TISSUE ENGINEERING: Part A
Volume 16, Number 9, 2010

DOI: 10.1089/ten.tea.2010.0090

Mimicking Natural Dentin Using Bioactive Nanohybrid Scaffolds for Dentinal Tissue Engineering

Ana Vallés-Lluch, Ph.D.,[1,2] Edurne Novella-Maestre, Ph.D.,[3] María Sancho-Tello, Ph.D.,[3] Manuel Monleón Pradas, Ph.D.,[1,2,4] Gloria Gallego Ferrer, Ph.D.,[1,2,4] and Carmen Carda Batalla, Ph.D.[3]

Synthetic materials mimicking the internal porous structure of natural dentin were prepared as nanohybrid matrix scaffolds made of poly(ethyl methacrylate-co-hydroxyethyl acrylate), pure and with a sol-gel-derived interpenetrated silica nanophase, with aligned tubular pores in the micrometer range typical of dentinal tissue. Some of them were internally coated with a layer of hydroxyapatite by immersion in simulated body fluid. Their physicochemical and mechanical properties were investigated. The different types of scaffolds were implanted subcutaneously into immunocompromised nude mice for 4, 6, and 8 weeks and their biological response were analyzed. Optical microscopy was employed to study the scaffold structure and neovascularization. Cells origin, inflammation, and macrophagic responses were evaluated by optical microscopy, immunohistochemistry, and transmission electron microscopy. The scaffold ultrastructural pattern imitates dentinal histological structure. The materials allowed cell colonization and neoangiogenesis. These biomaterials were colonized by murine cells fenotypically different to those of dermal connective tissue, showing structural differentiations. Colonization and viability were improved by the use of mineralized interphases, which showed a cellular distribution resembling a neodentinal pattern. Invasion of the scaffold tubules by single odontoblast-like processes was ascertained both in the noncoated and coated scaffolds. Such materials thus seem promising in tissue engineering strategies for dentin regeneration.

Introduction

Dentin is the mineralized tissue beneath enamel and *cementum* that constitutes the tooth body. It provides a cover for the pulp and serves as a support for the overlying highly mineralized enamel while compensating for its brittle nature. Without the support of the dentin structure, enamel would fracture when exposed to mastication forces. One of the morphological features of dentin is the presence of small tubules with a few micron diameter, which cross it from the pulp chamber to the region just below the dentin–enamel junction. Each tubule contains the apical prolongation of one odontoblast,[1,2] whose cell bodies are located at the base of the tubules, forming the peripheral boundary of the pulp.[3]

Dentin is a composite structure formed by ~30 vol% of an organic matrix, consisting mainly of type I collagen, a 50 vol% of an inorganic reinforcing phase of carbonated apatite and a 20 vol% of dentinal fluid similar to blood plasma. The mineral constituent of dentin is a carbonate-rich calcium-deficient hydroxyapatite (HAp).[4]

Odontoblasts, as highly differentiated cells, have lost the ability for mitosis and self-reproduction,[5] but since they can be stimulated to deposit more dentin, this tissue is capable of a limited repair.[1,3] Besides, the number of pulp progenitor/stem cells in a permanent tooth is not large enough for tooth regeneration.[6] Consequently, dentin does not remodel continuously as bone does, but responds to injuries by forming a kind of reactive dentin to protect the dental pulp.[7]

The conventional techniques employed for caries treatment involve the removal of the pulp tissue to avoid an inflammatory reaction and to preserve the surrounding tissues to prevent tooth loss, and the replacement of the affected dental tissue by synthetic filling composites and sealing it up, to minimize the possibility of bacterial recolonization and avoiding tissue fluids to seep inside the tooth.[2,8] Few of these materials share the same physical or chemical characteristics of the natural replaced tissue, and thus these cavity restorations tend to fail mechanically. Besides, microleakage at the composite–tooth interface with the penetration of bacterial enzymes, bacteria, fluids, and ions tends to produce hypersensitivity and secondary caries.[1,8]

[1]Center for Biomaterials and Tissue Engineering, Universidad Politécnica de Valencia, 46022, Valencia, Spain.
[2]Biomaterials Unit, Centro de Investigación Príncipe Felipe, 46013 Valencia, Spain.
[3]Pathology Department, Faculty of Medicine and Odontology, Universidad de Valencia, Spain.
[4]Networking Research Center on Bioengineering, Biomaterials and Nanomedicine (CIBER-BBN), Valencia, Spain.

An ultimate goal in dental therapies would be to maintain not only structure but also vitality and function of the dentinal–pulp complex, by stimulating dentinogenic response and restoring the cavity with healthy tissue. In the last years, different tissue engineering strategies for tooth tissues have been proposed.[2,8–13] Some of them are based on the stimulation of pulpal progenitor cells to differentiate to odontoblasts,[8] either by (1) enhancing the natural healing potential of pulp tissue by application of bone morphogenetic proteins, or by (2) *ex vivo* isolation of stem cells, differentiation, and transplantation, when there is severe inflammation and few stem cells in the dental pulp. A third strategy aims at (3) inducing the regeneration of tooth structures by means of cell–scaffold constructs, where the prefabricated natural or synthetic scaffold works as extracellular matrix for adhesion, proliferation, and differentiation of cells.[8,13] Buurma *et al.*[9] implanted nonwoven polyglycolic acid (PGA) fiber scaffolds, previously seeded and cultured with human dental pulp fibroblasts (HPF), into subcutaneous sites in immunocompromised mice. They found that these HPF survived and synthesized type I collagen and cellular fibronectin (FN) and expressed genes implicated in transducing bone morphogenetic protein signals. Young *et al.*[10] and Yelick and Vacanti[12] seeded different spongeous biodegradable scaffolds of polylactic acid and PGA with cell suspensions obtained from dissociated porcine tooth buds, and later on they implanted them in the omenta of athymic rats. The scaffolds provided a support into which epithelial (enamel producing) and mesenchymal (dentin and pulp producing) dental cells could interact and differentiate. Their histological analyses revealed the regeneration of the two major mineralized structures of the tooth: dentin and enamel. The formation of many small tooth crowns randomly orientated instead of one large bioengineered tooth with the shape of the scaffold was attributed to the heterogeneity of tooth bud cell populations. In this context, Honda *et al.*[14] hypothesized that if the contact positions between the epithelial and mesenchymal cells could be manipulated during the initiation of tooth regeneration, the tooth morphology would be regular in shape. They separated and dissociated mesenchyme and epithelium from porcine third molar teeth; then, they seeded mesenchymal cells onto the surface of spongeous natural collagen scaffolds and epithelial cells on top, so that the two cell types were in direct contact, and implanted the cell–scaffold constructs into immunocompromised rats. After 20 weeks, the implants acquired the structural characteristics of teeth with mineralized dentin, odontoblasts lining the inner surface of the predentin matrix and ameloblasts adjacent to a small amount of enamel, in contrast with abnormal shapes generated by random seeding of cells onto the scaffolds. These results indicated that direct cell–cell contacts were necessary for enamel–dentin regeneration. Bohl *et al.*[2] demonstrated that PGA scaffolds were more efficient than collagen or alginate scaffolds when cultured *in vitro* with seeded HPF. In another approach, Young *et al.*[15] prepared hybrid tooth–alveolar bone foam scaffolds of PGA and polyglycolide-*co*-lactide for the clinical treatment of tooth loss accompanied with alveolar bone resorption. On the one hand, tooth scaffolds of these materials were seeded with pig tooth bud cells and cultured *in vivo* for 10 days in the omenta of adult rat hosts; on the other, bone scaffolds were seeded with osteoblasts from bone marrow progenitor cells and grown in a bioreactor. Once harvested, the scaffolds were sutured together and reimplanted. Eight weeks after reimplantation, the tooth–bone hybrid constructs showed primary and reparative dentin in the tooth portion, osteocalcin, and bone-sialoprotein-positive bone in the bone portion, and type III collagen–positive connective tissue resembling periodontal ligament and tooth root structures at the interface.

Among nonbiodegradable synthetic materials, those most frequently used for preparing scaffolds were calcium phosphates (HAp, β-tricalcium phosphate, and their derivatives). Wang *et al.*[16] cultured human dental pulp cells onto calcium polyphosphate scaffolds for 14 days and found good adhesion, proliferation, and spreading of the cells within the scaffolds. Many fine processes and matrix secretory granules could be seen on cell surfaces, suggesting differentiation of the seeded cells into functional odontoblast-like cells. Zhang *et al.*[17] followed the reaction of human dental pulp stem cells on different scaffold materials: a spongeous collagen, a porous sintered HAp/tricalcium phosphate, and a fibrous titanium mesh. All of them supported the attachment, growth, and differentiation of pulpal stem cells *in vitro*, but only little amounts of hard tissue were formed in *in vivo* subcutaneous experiments in immunocompromised rats, compared to those formed in similar materials but using bone marrow cells. Yoshikawa *et al.*[18] decided to use bone marrow mesenchymal cells for their experiments to avoid the undesirable extirpation of autologous odontoblasts (limited by the accessibility and availability of sufficient donor tissue). They found bone formation in HAp scaffolds seeded with bone marrow cells from rat femurs after 4 weeks of *in vivo* subcutaneous implantation in rats, but only if the scaffolds were previously coated with hyaluronic acid, which promoted cell differentiation and bone formation in the pores. However, they did not find a significant difference in bone formation with and without hyaluronic acid in *in vitro* monolayer cultures.

Although these results with spongeous or fiber scaffolds as synthetic tooth tissues show some promising results, these materials did not exhibit mechanical or physical properties similar to natural tooth tissues, the scaffolds did not mimic the natural architecture of the dental structures, and the compatibility of the materials with the surrounding mineralized tissues was not evaluated. Therefore, the aim of the present study was to address some of these issues.

Here we have investigated the cellular colonization of synthetic matrices based on hybrid organic–inorganic nanocomposites mimicking the structure and properties of the mineralized matrix tissue of natural dentin. Considerations of two kinds lead to the choice of composition for the organic matrix. On one hand, the material should possess enough mechanical strength in compression; on another hand, it should also possess a degree of hydrophilicity. In this way, one expects the material to withstand mastication forces and to be easily invasible by body fluids. Thus, a two-component combination was chosen, the comonomer ethyl methacrylate (EMA) providing for mechanical strength but being hydrophobous, and the comonomer hydroxyethyl acrylate (HEA) providing for hydrophilicity. A weight ratio of 70:30 was chosen in the present study, and seen to guarantee a correct value of compressive modulus.[19] Silica has been found to produce a reinforcing effect in this organic matrix,[19,20] while at the same time it confers bioactivity to the surfaces.[21] The

obtained porous structures are expected to stimulate the invasion by odontoblast prolongations of the scaffold pores when implanted *in vivo*, which would be able to synthesize new natural dentin while providing a good adhesion between the scaffold and the surrounding natural tissue.

Materials and Methods

Preparation of the scaffolds

Microtubular porous scaffolds were prepared by polymerization of two types of reactant mixtures in the presence of a fiber template inside a tubular mold. Two types of scaffolds were prepared: scaffolds of the copolymer poly(ethyl methacrylate-*co*-hydroxyethyl acrylate), P(EMA-*co*-HEA), and scaffolds of the same copolymer with a 15 wt% of simultaneously sol-gel polymerized silica, SiO_2. Briefly, EMA monomer (99%; Aldrich) and HEA monomer (96%; Aldrich), in a 70/30 wt% monomer ratio, were mixed together with a 0.5 wt% of ethylene glycol dimethacrylate (98%; Aldrich), as crosslinking agent, and a 2 wt% of benzoyl peroxide (97%; Fluka), as thermal initiator, relative to monomer weight (reactive mixture I). Separately, a solution was prepared by mixing tetraethoxysilane (98%; Aldrich) with distilled water and hydrochloric acid (37%; Aldrich) in the molar ratio 1:2:0.0185, respectively, which was then mixed with the reactive mixture I in a mass proportion such as to render a 15% in weight of silica, by controlling the (EMA+HEA)/tetraethoxysilane ratio and assuming completion of silica polymerization sol-gel reactions (reactive mixture II). Glass tubes of 3-mm inner diameter were cut into 3.5-cm-long pieces, stuffed with 10-μm-diameter polyacrylonitrile (Montefibre) aligned fibers and sealed on one side. The previously prepared reactive mixtures were vacuum-injected in these glass molds: the mixture I for the scaffold termed hereafter H00, with P(EMA-*co*-HEA) matrix; the mixture II for the scaffold hereafter termed H15, with hybrid P(EMA-*co*-HEA)/SiO_2 nanocomposite matrix. The tubes were immediately capped and placed in an oven for polymerization at 60°C for 21 h followed by postpolymerization at 90°C for 18 h. Afterward, the polyacrylonitrile fibers were eliminated from the materials by dissolution in *N*,*N*-dimethylformamide (99.8%; Aldrich). The resulting scaffolds were washed in ethanol to remove residuals and unreacted monomers, and finally dried in a vacuum desiccator at 80°C until constant weight. In this way, scaffolds of P(EMA-*co*-HEA) (H00) and P(EMA-*co*-HEA) with 15 wt% of SiO_2 (H15) with aligned tubular pores were obtained.

HAp coating

The ability of the H15 scaffolds to nucleate HAp on their surfaces was tested *in vitro*, by soaking them in a simulated body fluid (SBF) solution with ion concentrations nearly equal to those of the human blood plasma, by the method proposed by Kokubo and coworkers.[22,23] To obtain the SBF, two solutions were prepared. Solution 1 comprised 1.599 g of NaCl (99%; Scharlau), 0.045 g of KCl (99%; Scharlau), 0.110 g of $CaCl_2{\cdot}6H_2O$ (99%; Fluka), and 0.061 g of $MgCl_2{\cdot}6H_2O$ (Fluka) in deionized ultra-pure water (Scharlau) up to 100 mL. Solution 2 was prepared by dissolving 0.032 g of $Na_2SO_4{\cdot}10H_2O$ (Fluka), 0.071 g of $NaHCO_3$ (Fluka), and 0.046 g of $K_2HPO_4{\cdot}3H_2O$ (99%; Aldrich) in water up to 100 mL. Both solutions were buffered at pH 7.4, by adding the necessary amounts of aqueous 1 M tris-hydroxymethyl aminomethane, $(CH_2OH)_3CNH_2$ (Aldrich), and 1 M HCl (37%; Aldrich). Then, both solutions were mixed to obtain SBF with the following molar ion concentrations (in mM): 142 Na^+, 5.0 K^+, 1.5 Mg^{2+}, 2.5 Ca^{2+}, 148.8 Cl^-, 4.2 HCO_3^-, 1.0 HPO_4^{2-}, and 0.5 SO_4^{2-}.

Pieces of scaffolds of 3 mm length were suspended from a cotton thread inside closed glass vials filled with SBF. The ratio of geometric surface area of scaffold (without considering the inner pores surface) to solution volume was 0.12 mL/mm^2. The SBF solution was not renewed during the first 7 days. After the seventh day, a 2× SBF solution (with ion concentrations adjusted to twice those of SBF) with renovation was employed. This solution was renewed each 2–3 days, to provide more favorable conditions for HAp deposition.[24–26] Samples were withdrawn from the SBF after 7 (hereafter referred to as H15HAp7 scaffolds) and 14 days (hereafter referred to as H15HAp14 scaffolds), rinsed with water, room conditioned, and finally dried in a vacuum desiccator at 80°C.

Characterization of the scaffolds

Morphological analysis of the scaffolds was undertaken by scanning electron microscopy (SEM), in a JSM-6300 microscope (JEOL), with the samples previously sputter-coated with gold, 15 kV of acceleration voltage, and 15 mm of working distance. SEM images were obtained in both longitudinal and transversal sections.

The quantification of silica and the compositional changes occurring during the test in SBF were elucidated by microanalysis in an energy dispersive X-ray spectrometer (EDS) from Oxford Instruments, attached to the scanning electron microscope. Samples were previously sputter-coated with carbon under vacuum. Spectra were taken at 10 kV of acceleration voltage and 15 mm of distance working. Silicon was employed as optimization standard.

The porosity of the scaffolds (pore volume fraction in the scaffold), π, was calculated through the density of the respective bulk samples, obtained elsewhere,[20] and the weight and total volume of the scaffolds (calculated geometrically), in duplicate. A Mettler AE 240 balance (Mettler-Toledo) with a sensitivity of 0.01 mg was used. The following equation was employed:

$$\pi = \frac{V_{pores}}{V} = \left(1 - \frac{m_{scaff}/\rho}{V}\right) \cdot 100$$

where V_{pores} is the volume of the sample occupied by pores, V is the overall sample volume, ρ is the density of the material making the sample, and m_{scaff} is the weight of the scaffold.

The swelling of the samples in water was quantified by weighing the samples dried and after equilibration to constant weight immersed in distilled water at 37°C using the previously mentioned balance. A constant value of the weight was attained in around 96 h. Measurements were repeated three times for each composition. The equilibrium water contents (EWC) is defined as the ratio between the mass of water in the sample, m_{water}, and the mass of the dry sample, m_{dry}:

$$EWC = \frac{m_{water}}{m_{dry}}$$

Mechanical compression assays were performed in the longitudinal, axial direction (the tubular pores in the vertical

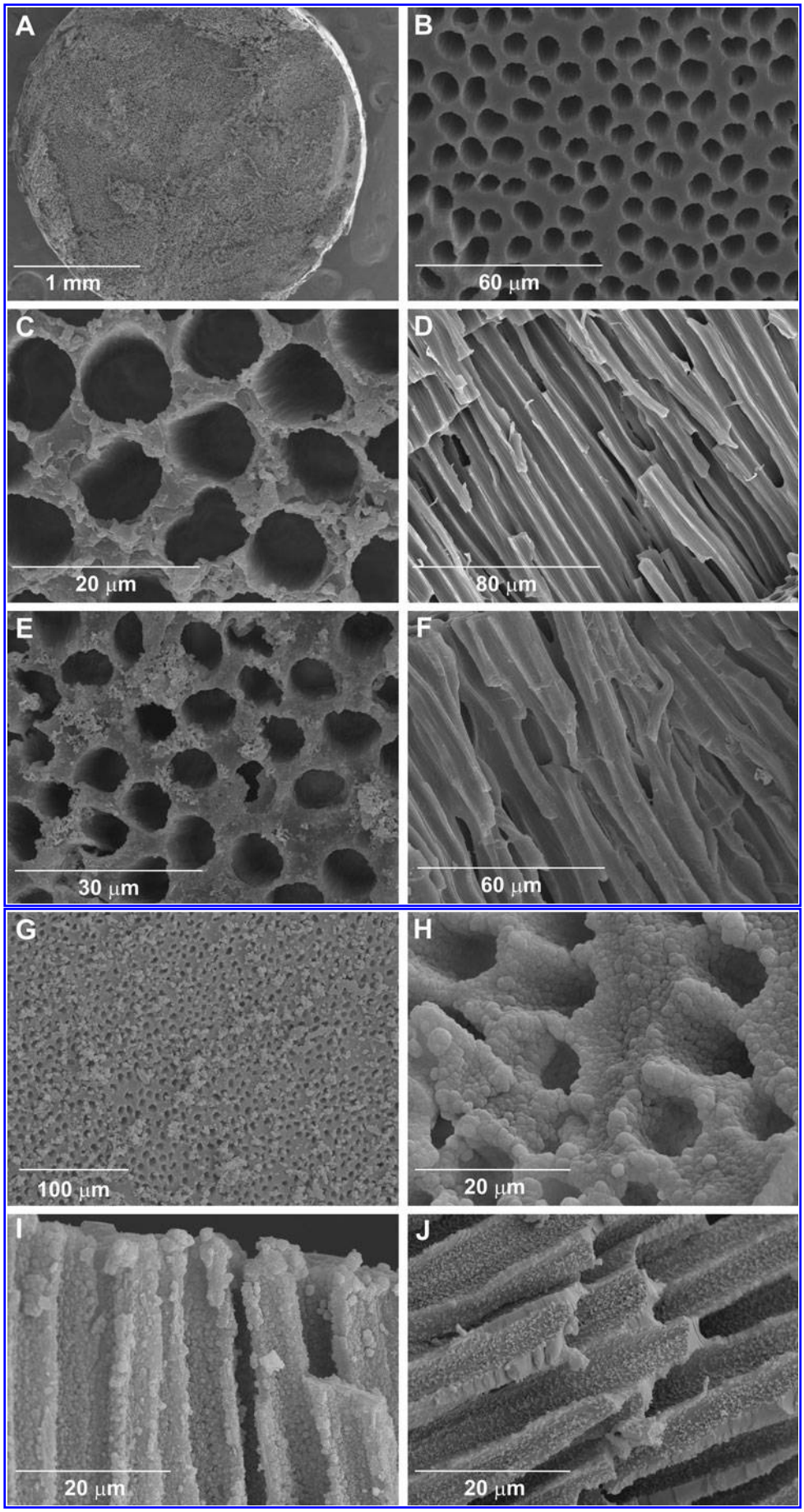
A
1 mm
B
60 μm
C
20 μm
D
80 μm
E
30 μm
F
60 μm
G
100 μm
H
20 μm
I
20 μm
J
20 μm

direction, which will be their position when the scaffold is implanted in the tooth) in a Seiko TMA/SS6000 equipment (Seiko Instruments), from 0 to 150 g, at a 10 g/min loading rate, on the dry scaffolds at room temperature and also on the scaffolds equilibrated in distilled water at 37°C. Measurements were repeated three times for each composition. Samples were cylindrical, 3 mm in diameter, and ~3 mm in height.

Subcutaneous implants in vivo

This study was performed using procedures approved by Real Decreto 223/1988 March 14th about animal protection in experimentation, Directive 86/609/CEE, November 14th, 1986. The animals were conducted in accordance with the NIH guidelines for the care and use of laboratory animals. Protocols for animal handling were approved by the ethics committee of the Valencia University School of Medicine and Odontology.

Animals

The homozygous nude mouse mutants (nu/nu) with a congenital thymus aplasia, resulting in a deficient T-lymphocyte system[27] were used. Male nude mice (Balb/c, IFA-CREDO), 4 weeks old, were individually housed in autoclaved cages and bedding, in laminar flow filtered hoods. The animal room was maintained at 26°C with a 12-h light–12-h dark cycle, and mice were fed *ad libitum* with autoclaved laboratory rodent chow and acidified water. All handling was performed in laminar flow filtered hoods. A mixture of ketamine (Ketolar®; Parke-Davis)/medetomidine (Domtor®; Pfizer) (75 μg/g ketamine and 1 μg/g medetomidine) intraperitoneally injected was used to anesthetize mice before invasive procedures, and atipemazol (Antisedan®; SmithKline Beecham) 1 μg/g intraperitoneal, to reverse the anesthesia effects, was employed after invasive procedures, using sterile instruments.

Scaffolds subcutaneous xenotransplantation

Scaffold samples of P(EMA-*co*-HEA) (H00), P(EMA-*co*-HEA)/15 wt% SiO_2 (H15), and P(EMA-*co*-HEA)/15 wt% SiO_2 with the tubular surface coated with HAp during 14 days in SBF (H15HAp14) were implanted subcutaneously into the backs of 10 4-week-old Balb/c male nude mice. Half of the scaffolds were immersed in an FN solution (0.1% solution from bovine plasma; Sigma) overnight before the implantation. Mice were sacrificed after 4, 6, and 8 weeks.

Optical microscopy study

Material for optical study was fixed in 4% neutral buffered formalin, before being routinely paraffin wax embedded and cut into 4 μm serial sections. Four to five noncontiguous sections from each specimen were stained with Harris's hematoxylin and eosin (Sigma) and examined microscopically.

Ultrastructural study by transmission electron microscopy

Specimens for ultrastructural study were fixed in 2.5% glutaraldehyde (buffered at pH 7.4 in Sorensen phosphate solution) immediately after extraction. Then, tissues were postfixed for 2 h in 1% osmium tetroxide in buffer and after dehydration with graded concentrations of acetone, the tissue blocks were embedded in Epon 812 (TAAB Lab). Semithin Epon sections (1 μm) were stained with toluidine blue for control in a light microscope and trimmed for ultrastructural study. Ultra-thin sections were cut with a diamond knife using a Reichert ultramicrotome (Leica), contrasted with uranyl acetate and lead citrate, and examined in a JEOL JEM-1010 (JEOL) transmission electron microscope at 60 kV.

Immunohistochemistry

Four-micron serial sections of the xenotransplanted scaffolds were subjected to standard immunohistochemistry. Sections were deparaffinized and rehydrated through graded ethanol, rinsed in distilled water, and treated with 0.3% H_2O_2 and 10% normal horse serum to block endogenous peroxidase and nonspecific binding, respectively. Antigen retrieval was performed by pressure cooker boiling for 3 min in 10 mmol/L of citrate buffer (pH 6.0).

A rabbit anti-mouse CD11b antibody (ABR-Affinity Bioreagents) at 1:25 dilution, incubated at room temperature for 60 min, was employed to specifically detect the possible macrophagic, monocytic, and granulocytic adhesion processes inside the xenotransplanted scaffolds, and mouse central nervous system tissue was used as positive control. A monoclonal rat anti-mouse CD-31 antibody (Abcam) at 1:100 dilution, incubated at room temperature for 60 min, was employed to specifically detect the incipient angiogenic processes inside the scaffolds and mouse kidney tissue was used as control. Biotinylated goat anti-rat (Serotec) at 1:50 dilution incubated at room temperature for 30 min was employed as the secondary antibody. The standard immunohistochemistry staining method labeled streptavidin biotin (LSAB) method (DakoCytomation) was used, followed by detection with 3,3-diaminobenzidine. As a negative control for each specific staining, the preimmune serum was substituted for the primary antibody.

Results

Characterization of the scaffolds

The transversal sections of H00 (Fig. 1A, B) and H15 (Fig. 1C, D) scaffolds showed a homogeneous distribution of cylindrical pores of ~8 μm of diameter in all cases. Neither

FIG. 1. Morphology of the scaffolds as seen by scanning electron microscopy. The sections of P(EMA-*co*-HEA) (H00) (**A, B**) and P(EMA-*co*-HEA)/15 wt% SiO_2 scaffolds (H15) (**C, D**) presented a homogeneous distribution of cylindrical pores. Scanning electron microscopy images of 7-day HAp-coated P(EMA-*co*-HEA)/15 wt% SiO_2 (H15HAp7) scaffolds presented some scattered deposits but nothing in the interior surfaces of the pores (**E, F**), while after 14 days (H15HAp14) formed cauliflower patterns typical of bioactive glasses (**G–J**). (**A–C, E, G, H**) Transversal sections. (**D, F, I, J**) Longitudinal sections. P(EMA-*co*-HEA), poly(ethyl methacrylate-*co*-hydroxyethyl acrylate); HAp, hydroxyapatite.

the pore diameter nor their distribution seemed to vary with the composition.

The density of the bulk materials increased from 1.17 g/cm^3 for H00 to 1.25 g/cm^3 for H15.[20] The porosity of the obtained H00 scaffolds was 37.26% and that of H15 scaffolds increased to 52.25%, but it could be modulated by employing different amounts of porogen fibers inside the glass tubes.

H15 hybrid scaffolds after 7 days in SBF (H15HAp7) showed only some scattered deposits in the transversal section, but nothing in the interior surfaces of the pores (Fig. 1E, F). By contrast, the H15 hybrid scaffolds after 14 days in SBF (H15HAp14) showed needle-shaped HAp polycrystals covering the external transversal surface (Fig. 1G, J), forming cauliflower structures, with an average diameter of 1 μm, which did not occlude the pores cavities. As a consequence, the average tubule diameter decreased from 8 to ~5 μm. Scattered aggregates of cauliflowers with larger diameter, of what seem to be subsequent layers, were superposed to the first homogeneous coating. The longitudinal fractures showed that the surface of the tubular pores was almost completely coated after 14 days in SBF in the regions near the ends, but somewhat less in the inner zones.

The silica contents in the H15 scaffold (calculated from the experimentally measured EDS Si average contents) was 15.33% in the bulk and 15.09% at the surface; that is, they correlated very well with the nominal silica content (Fig. 2). In the case of H15HAp14, Si could not be detected by EDS; instead, Ca and P were the main elements, and other elements like Na and Cl were also detected (Fig. 2). The average Ca/P ratio calculated by EDS was 1.56.

The EWC of the H00 scaffolds was 7.67%, and that of the H15 scaffolds was 7.35%. The EWC was also referred to the mass of the hydrophilic component of the copolymer, HEA, by defining a reduced water content (EWC′) as

$$EWC' = \frac{m_{water}}{m_{HEA}} = \frac{m_{water}/m_{dry}}{m_{HEA}/m_{dry}} = \frac{EWC}{x_{HEA}}$$

where x_{HEA} is the mass fraction of HEA in the sample and EWC is the EWC referred to the dry mass of the sample. Referred to the HEA mass in the sample, the EWC was 25.57% for H00 and 28.82% for H15.

The compressive elastic moduli of the scaffolds were obtained from the slope of the stress–strain curves of the compressive tests performed in the axial direction. The elastic modulus of the dry H00 scaffolds was 3685 MPa and that of H15 increased to 6156 MPa. The compressive elastic modulus of the H15HAp14 scaffolds was 8192 MPa, 1.33-fold that of the original H15 scaffolds. With regard to the scaf-

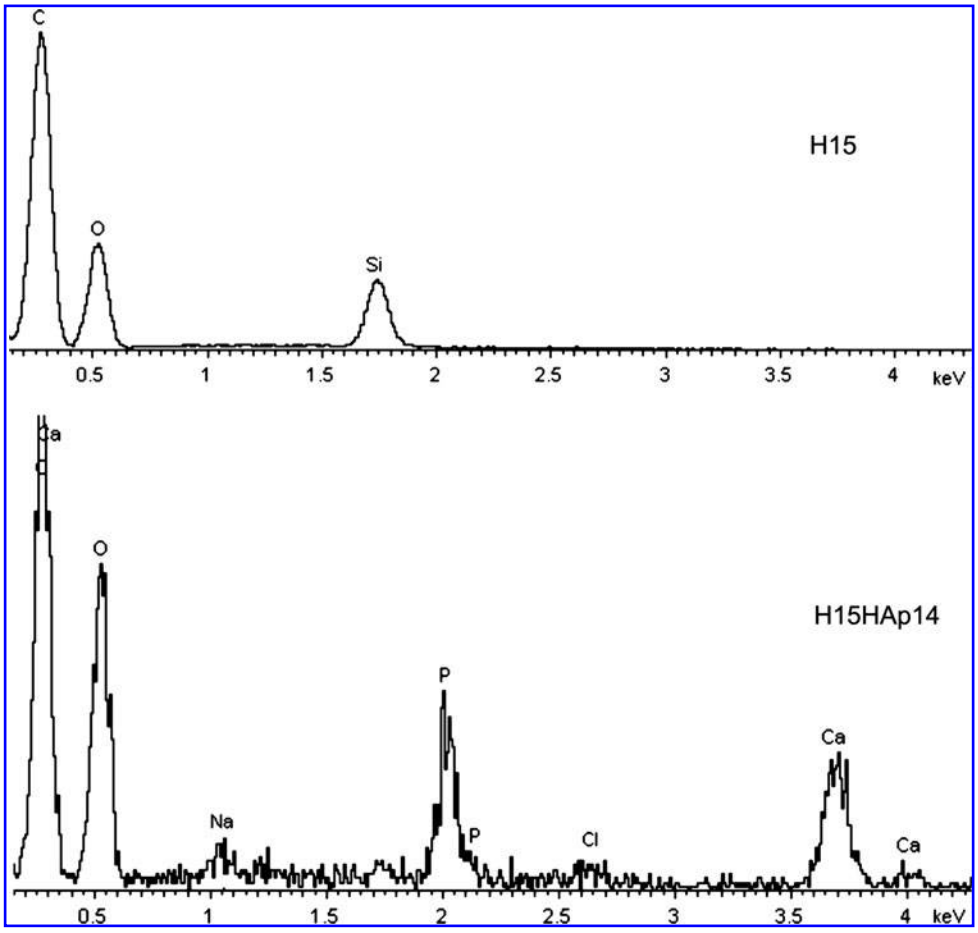

FIG. 2. Energy-dispersive X-ray spectra of the P(EMA-*co*-HEA)/15 wt% SiO_2 scaffold (H15) and the 14-days HAp-coated P(EMA-*co*-HEA)/15 wt% SiO_2 scaffold (H15HAp14).

folds equilibrated in water at 37°C, the modulus of H00 decreased to 680 kPa and that of H15 to 1749 kPa.

Biological response

The histological study of the H00 (Fig. 3A, B) and H15 (Fig. 3C) explanted scaffolds revealed a good cellular colonization of the areas occupied by the materials and an intense neoangiogenesis around them, which was increased when the scaffolds were previously coated with FN (Fig. 3B). H15HAp14 scaffolds (Fig. 3D) showed the best cellular distribution and neo-dentinal pattern. In this case the presence or absence of FN did not modify the results. Cellular nesting decreased after 4 weeks in the H00 and H15 scaffolds, whereas it was stable until 8 weeks in H15HAp14 samples (Fig. 3D).

Elements with intense CD11b immunostaining were observed in the areas surrounding the scaffolds, whereas the elements located inside of the tubules were not positive for that stain (Fig. 3E). The explants presented a rich vascular net, which penetrated inside the dentinal-like tubules: the immunohistochemical study with CD31 demonstrated abundant blood vessels inside the scaffold (Fig. 3F).

The cellular typification by transmission electron microscope is shown on Figures 4 and 5. Cell colonization of the scaffolds was markedly different in each type of structure, changing the number of elements that invaded the dentin neo-matrix. The cells in the H00 scaffolds adopted a pattern with reticular appearance (Fig. 4A). Cellular characterization revealed cells with immature fibroblastic characteristics (mesenchymal-like). In the case of nonmineralized H15 scaffolds, the nested cells located in the center of the scaffolds showed a mild cytoplasmic differentiation along with a high quantity of collagen surrounding the cellular net (Fig. 4B).

At the ultrastructural level, H15 and H15HAp14 scaffolds displayed a dentin-like pattern, with single cellular prolongations included in the tubules (Fig. 5A). In some cases, a pattern imitating reactive dentin was observed, showing also the cytoplasm and nucleus within the tubules (Fig. 5B, C). These cells had a markedly secretory character, but with smaller amount of collagen in the mineralized

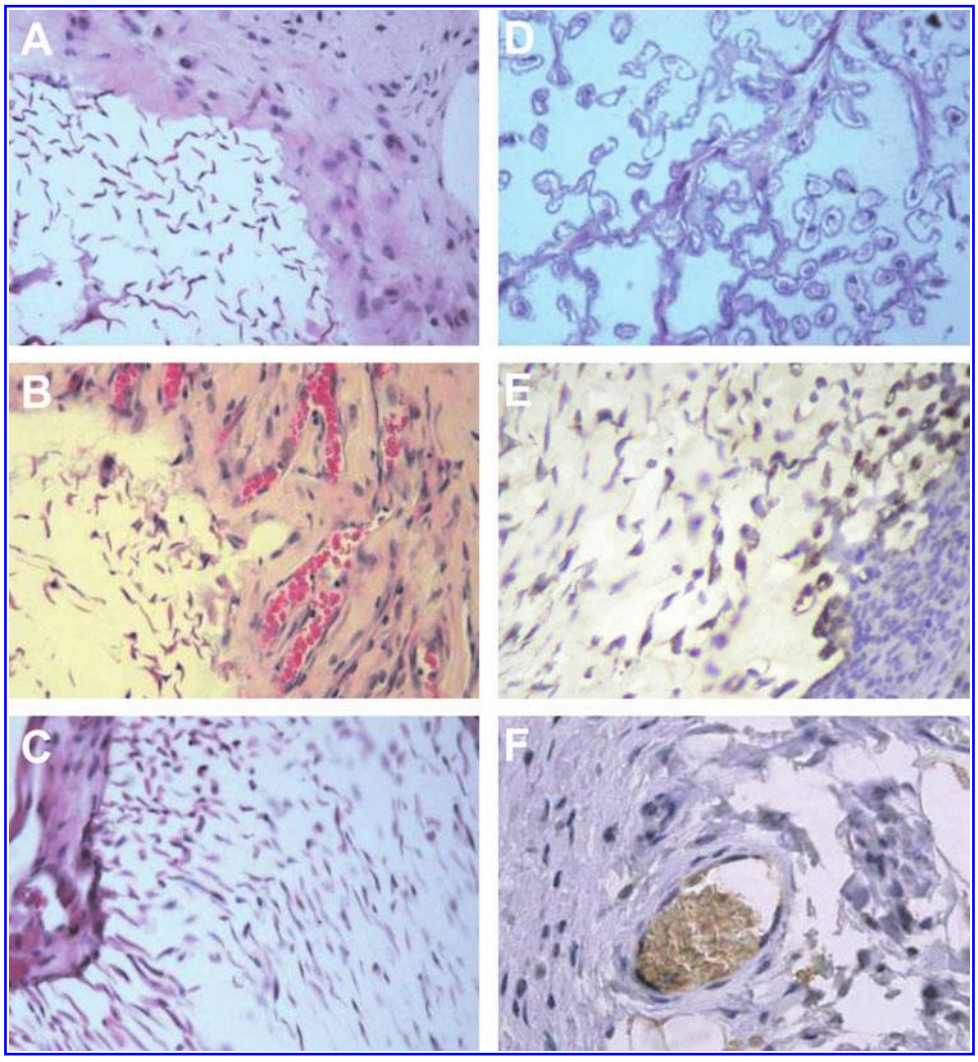

FIG. 3. (**A**) H00 scaffolds presented a good cellular distribution pattern, with cells totally different to murine stromal cells. (**B**) Intense neoangiogenesis process improved by fibronectin was observed in the same group. (**C**) Histologies of H15 scaffolds after 4 weeks presented a tubular pattern. (**D**) Transversal section of H15HAp14 scaffolds showed a better structural pattern much more similar to the tubular dentin matrix, with dentinal pattern and imitating in some cases a reactive dentin. (**E**) In the surrounding areas of H15HAp the existence of elements with an intense CD11b immunostain was ascertained, while the elements located inside of the tubules did not show immunostain. (**F**) Immunomarker CD31 demonstrated abundant blood vessels inside the H15HAp scaffold. (**A–C**) Four weeks, hematoxylin–eosin, original magnification 40×. (**D**) Eight weeks, hematoxylin–eosin, original magnification 60×. (**E, F**) Eight weeks, original magnification 60×. Color images available online at www.liebertonline.com/ten.

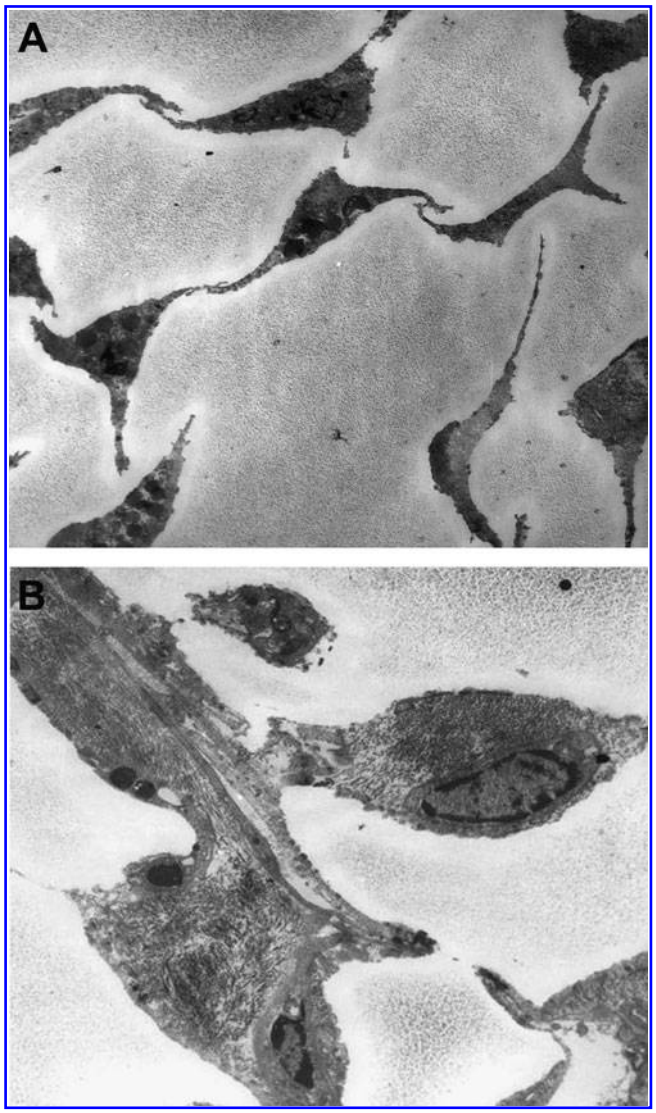

FIG. 4. TEM image of H00 scaffold with cellular reticular cell pattern (original magnification 800×) (**A**). TEM images of H15 scaffold with intense matrix synthesis (2500×) (**B**). TEM, transmission electron microscope.

scaffolds, probably due to narrower tubules with mineralized walls (Fig. 5A–C).

Discussion

Scaffolds of P(EMA-*co*-HEA) 70/30 wt%, pure and with 15 wt% SiO_2, were successfully produced by means of a procedure involving a simultaneous polymerization of the organic and inorganic matrices and a fiber templating method, to yield homogeneously distributed, aligned tubular pores of 8 μm of diameter within a bioactive, nanocomposite hybrid matrix. These synthetic scaffolds resemble natural dentin with regard to the structure and distribution of the pores and the mechanical properties. The composition of these materials includes a component responsible for the high mechanical properties (EMA), a bioactive component (silica), and a hydrophilic monomer (HEA), responsible for the good permeability to body fluids of the composite. The fact that the hydrophilicity of the H15 scaffolds, as measured by EWC′, is slightly higher than that of the H00 scaffolds must be attributed to the additional effect of the hydroxyl groups of silica.

A uniform coating of the pore surfaces by nucleated HAp required immersion in SBF up to 14 days; the progress of this process could be followed, and is reflected in the differences exhibited by the samples H15HAp7 (7 days in SBF) and H15HAp14 (14 days in SBF). The scaffolds were covered with needle-shaped HAp polycrystals forming cauliflower structures typical of bioactive glasses,[23,28–31] with an average diameter of 1 μm. The HAp-coating decreased the average tubule diameter to ∼5 μm. This new pore diameter resembles more that of the natural dentinal tubule, being thus more convenient for the proposed application.

EDS data confirmed the nominal silica contents of the nanohybrid matrices, and showed that after HAp coating in SBF, the surface did no longer expose silicon, but the components of the HAp: Ca and P were the main elements (other elements like Na and Cl were also detected), and the average Ca/P ratio was 1.56, similar but slightly lower than that of physiological HAp Ca/P ratio, which is 1.65,[25] or stoichiometric HAp,[23] 1.67. Because of the negligible weight increase due to the HAp coating, it was not possible to quantify the amount of HAp gravimetrically. Therefore, these EDS data and the SEM images were the best characterization of the apatite layer grown synthetically on the scaffolds' surfaces.

Sol-gel-derived nanocomposites yield two finely interpenetrated chemically independent networks: that of the organic copolymer and that of silica.[20] The silica network not only provides for the bioactivity (HAp nucleating ability) of the matrix, but also increases the compressive elastic modulus of the H15 with respect to that of the H00 scaffolds. An additional modulus increase is obtained as a consequence of the HAp coating. Even thus, our scaffold's modulus was still lower than that of human dentin, 14.47 GPa.[32] Nevertheless, when implanted *in vivo*, the regenerated mineralized tissue is expected to complement the material's modulus and trigger a self-adjusting process leading to a physiological compressive modulus.

The percentage of silica employed in this work for the *in vivo* assays was chosen on the basis of previous findings on bulk samples of P(EMA-*co*-HEA) 70/30 wt% with different silica percentages in the range 0–30 wt%.[19–21] In the hybrids with low silica contents, the silica nanodomains are uniformly interdispersed in the organic phase, and tend to aggregate into larger regions leaving spaces of tens of nanometers occupied by the organic network. Around a 15 wt% of silica, the inorganic network percolates and the nanodomains start to coalesce to form a co-continuous interpenetrated network. Above this silica content, the continuously extended dense silica network hinders the organic polymer network expansion and renders less nonreacted surface silanols. Therefore, nanohybrids with intermediate silica contents (10–20 wt%) exhibit an interesting balance between (1) good mechanical reinforcement due to an incipient percolating silica network, (2) swelling ability still not hindered by a too rigid silica skeleton, and (3) enhanced surface reactivity or bioactivity due to the still elevated relative contents of polar silanol terminal groups, since the bioactivity of silica implies its ability to dissolve.[21] The dissolution of silica at the surface is facilitated by the relatively

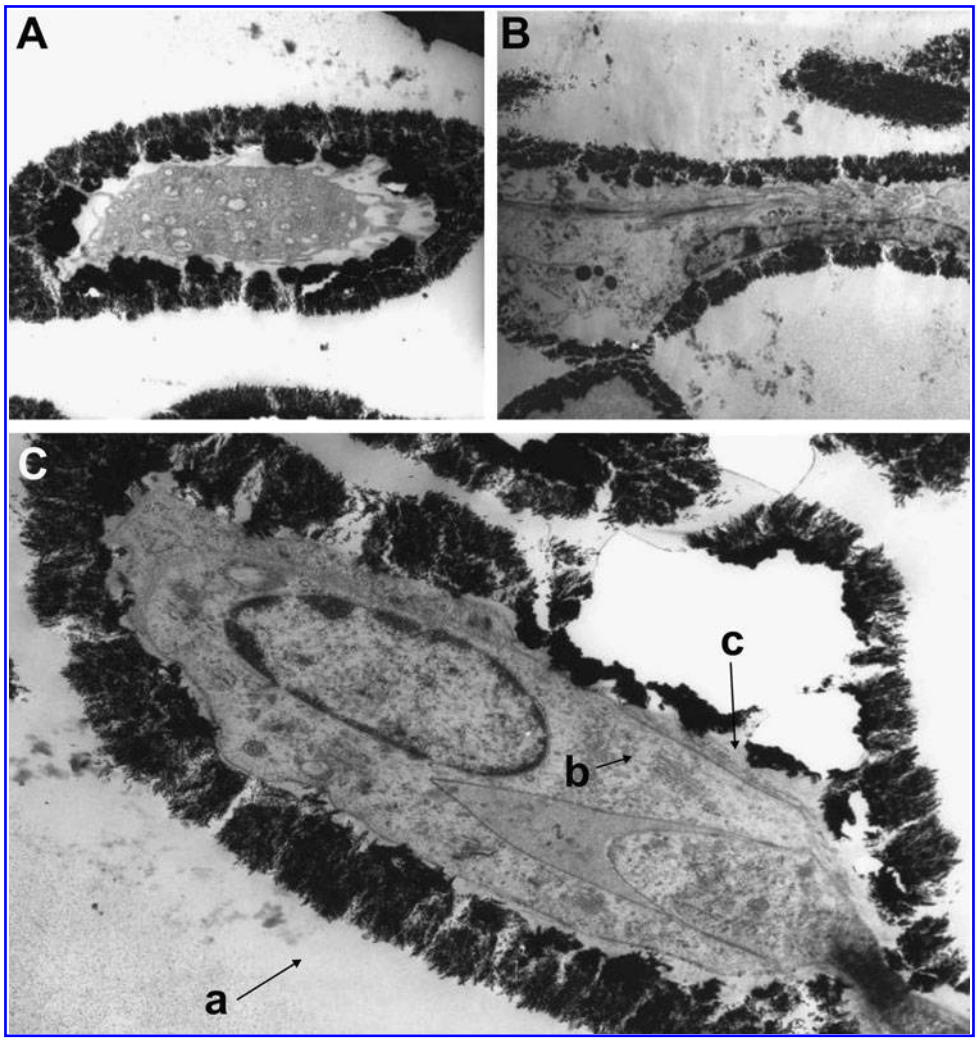

FIG. 5. TEM image of H15HAp14 scaffold explants presented a tubular pattern with lodged mesenchymal-secretory cells (3500×) within the tubules, where the cellular prolongations (**A**) and occasionally also the cytoplasm and nucleus (**B**, **C**) were observed. Cells showed a secretory character in the mineralized scaffolds, with the collagen surrounding the nested cells (**C**). Arrows: (a) scaffold, (b) cell, (c) collagen.

large number of noncondensed silanol terminal groups in the network due to the disconnected topology of the silica phase; as it dissolves, silica releases soluble silicates and renders an interface layer negatively charged rich in silanol groups. This reaction zone enhances electrostatic interaction with the positively charged calcium ions and next with the negatively charged phosphate ions in the SBF, leading to the formation of an amorphous calcium phosphate that crystallizes with time into HAp.[21]

When the scaffolds were xenotransplanted into immunodeficient mice, an active neoangiogenesis process was observed, along with a positive cellular colonizing response in all cases. There is an increase in the materials stiffness in the order H00 < H15 < H15HAp, which seems to be relevant for the observed differences in the organizational pattern of the cells that invade the synthetic structures. In the case of the softest hydrogel, scaffold H00, cells presented a network-like layout with slim collagen fibers, which is characteristic of pulpar tissue. The tubular pore structure of this scaffold could not be identified in the histological cuts (Figs. 3A, B and 4), nor were the cells that invaded it organized according to any recognizable tubular pattern. This was probably due to the early collapse of those pores, the material yielding to the pressure exerted by the surrounding tissue growth. By contrast, the highest modulus material, H15HAp, kept intact its tubular morphology and the cells that invaded it were organized in the typical dentinal, tubular-like, pattern (Figs. 3D and 5). Within these mineralized scaffolds, having a 15% of silica reinforcement besides an internal coating by a HAp layer, the cells presented a secretory character with cellular prolongations hosted in the tubules as in natural dentin. Occasionally, the cytoplasm and nucleus of cells were also found inside the tubules, imitating a reactive dentin. All these histological findings show that the structural pattern of these cell–scaffold constructs resembled the histological structure of the dentin, and encourage further *in vivo* investigations of this type of synthetic structures in models closer to the living tooth tissue.

Implants made of this material are being currently studied in drilled dental cavities of a dog experimental model, with the material in the shape of thin disks. Successfully validated results would open the possibility for use in humans as disks dimensionally shaped to fit prepared dentinal cavities after necrotic tissue removal, with the material acting as barrier to the progress of bacterial invasion and as scaffold for tissue regeneration.

Conclusions

A material structure (scaffold) has been developed that unites several features of interest for dentin replacement or regeneration: (1) it has a porous structure similar to that of the highly specialized dentin tissue; (2) it has compressive mechanical properties adequate to withstand physiological stresses in early healing stages; (3) it possesses bioactive surfaces and nucleates HAp when placed in physiological medium; (4) it is biocompatible and able to host single odontoblastic processes in its tubules. The matrix material is a hybrid nanocomposite with an organic phase of a P(EMA-*co*-HEA) copolymer and an inorganic phase of silica obtained by a simultaneous sol-gel polymerization process, which yields a finely interdispersed nanophase interpenetrated with the organic polymer phase. Subcutaneous *in vivo* test in nude mice revealed immunopatterns and ultrastructural differentiations similar to dentin structure. Cell colonization and viability were improved when the scaffolds had been premineralized *in vitro* and implanted with a HAp layer coating the pore surfaces, probably due to the increased stiffness of the material.

Acknowledgments

This work was in part supported by the 838/2007 grant from the Generalitat Valenciana. This work was partly financed through the "convenio de colaboración entre el Instituto de Salud Carlos III, la Conselleria de Sanidad de la Generalitat Valenciana y la Fundación de la Comunidad Valenciana Centro de Investigación Príncipe Felipe para la investigación básica y traslacional en medicina regenerativa."

Disclosure Statement

No competing financial interests exist.

References

1. Spencer, P., Wang, Y., and Katz, J.L. Dentin. In: Akay, M., ed. Wiley Encyclopedia of Biomedical Engineering. New Jersey: John Wiley & Sons, 2006, pp. 1051–1060.
2. Bohl, K.S., Shon, J., Rutherford, B., and Mooney, D.J. Role of synthetic extracellular matrix in development of engineered dental pulp. J Biomater Sci Polym Ed **9,** 749, 1998.
3. Walker, M.P., and Fricke, B. Dentin-enamel junction of human teeth. In: Akay, M., ed. Wiley Encyclopedia of Biomedical Engineering. New Jersey: John Wiley & Sons, 2006, pp. 1061–1064.
4. Marshall, G.W., Marshall, S.J., Kinney, J.H., and Balooch, M. The dentin substrate: structure and properties related to bonding. J Dent **25,** 441, 1997.
5. Zhang, W., Walboomers, X.F., Wolke, J.G.C., Bian, Z., Fan, M.W., and Jansen, J.A. Differentiation ability of rat postnatal dental pulp cells *in vitro*. Tissue Eng **11,** 357, 2005.
6. Yoshikawa, M., Tsuji, N., Toda, T., and Ohgushi, H. Osteogenic effect of hyaluronic acid sodium salt in the pores of a hydroxyapatite scaffold. Mater Sci Eng C **27,** 220, 2007.
7. Batouli, S., Miura, M., Brahim, J., Tsutsui, T.W., Fisher, L.W., Gronthos, S., *et al*. Comparison of stem-cell-mediated osteogenesis and dentinogenesis. J Dent Res **82,** 976, 2003.
8. Nakashima, M. Bone morphogenetic proteins in dentin regeneration for potential use in endodontic therapy. Cytokine Growth Factor Rev **16,** 369, 2005.
9. Buurma, B., Gu, K., and Rutherford, R.B. Transplantation of human pulpal and gingival fibroblasts attached to synthetic scaffolds. Eur J Oral Sci **107,** 282, 1999.
10. Young, C.S., Terada, S., Vacanti, J.P., Honda, M., Bartlett, J.D., and Yelick, P.C. Tissue engineering of complex tooth structures on biodegradable polymer scaffolds. J Dent Res **81,** 695, 2002.
11. Dobie, K., Smith, G., Sloan, A.J., and Smith, A.J. Effects of alginate hydrogels and TGF-β1 on human dental pulp repair *in vitro*. Connect Tissue Res **43,** 387, 2002.
12. Yelick, P.C., and Vacanti, J.P. Bioengineered teeth from tooth bud cells. Dent Clin North Am **50,** 191, 2006.
13. Murray, P.E., García-Godoy, F., and Hargreaves, K.M. Regenerative endodontics: a review of current status and a call for action. J Endod **33,** 377, 2007.
14. Honda, M.J., Tsuchiya, S., Sumita, Y., Sagara, H., and Ueda, M. The sequential seeding of epithelial and mesenchymal cells for tissue-engineered tooth regeneration. Biomaterials **28,** 680, 2007.
15. Young, C.S., Abukawa, H., Asrican, R., Ravens, M., Troulis, M.J., Kaban, L.B., *et al.* Tissue-engineered hybrid tooth and bone. Tissue Eng **11,** 1599, 2005.
16. Wang, F.M., Qiu, K., Hu, T., Wan, C.X., Zhou, X.D., and Gutmann J.L. Biodegradable porous calcium polyphosphate scaffold for the three-dimensional culture of dental pulp cells. Int Endodon J **39,** 477, 2006.
17. Zhang, W., Walboomers, X.F., van Kuppevelt, T.H., Daamen, W.F., Bian, Z., and Jansen, J.A. The performance of human dental pulp stem cells on different three-dimensional scaffold materials. Biomaterials **27,** 5658, 2006.
18. Yoshikawa, M., Tsuji, N., Toda, T., and Ohgushi, H. Osteogenic effect of hyaluronic acid sodium salt in the pores of a hydroxyapatite scaffold. Mater Sci Eng C **27,** 220, 2007.
19. Vallés-Lluch, A., Gallego Ferrer, G., and Monleón Pradas, M. Effect of the silica content on the physico-chemical and relaxation properties of hybrid polymer/silica nanocomposites of P(EMA-*co*-HEA). Eur Polym J **46,** 910, 2010.
20. Vallés-Lluch, A., Rodríguez-Hernández, J.C., Gallego Ferrer, G., and Monleón Pradas, M. Synthesis and characterization of P(EMA-*co*-HEA)/SiO_2 nanohybrids. Eur Polym J (in press, 2010, doi: 10.1016/j.eurpolymj.2010.04.010).
21. Vallés, A., Gallego, G., and Monleón, M. Biomimetic apatite coating on P(EMA-*co*-HEA)/SiO_2 hybrid nanocomposites. Polymer **50,** 2874, 2009.
22. Abe, Y., Kokubo, T., and Yamamuro, T. Apatite coating on ceramics, metals and polymers utilizing a biological process. J Mater Sci Mater Med **1,** 233, 1990.
23. Kokubo, T., and Takadama, H. How useful is SBF predicting *in vivo* bone bioactivity? Biomaterials **27,** 2907, 2006.
24. Tanahashi, M., Yao, T., Kokubo, T., Minoda, M., Miyamoto, T., Nakamura, T., *et al.* Apatite coating on organic polymers by a biomimetic process. J Am Ceram Soc **77,** 2805, 1994.
25. Kim, H.M., Kishimoto, K., Miyaji, F., Kokubo, T., Yao, T., Suetsugu, Y., *et al.* Composition and structure of the apatite formed on PET substrates in SBF modified with various ionic activity products. J Biomed Mater Res **46,** 228, 1999.
26. Oliveira, A.L., Malafaya, P.B., and Reis, R.L. Sodium silicate gel as a precursor for the *in vitro* nucleation and growth of a

bone-like apatite coating in compact and porous polymeric structures. Biomaterials **24,** 2575, 2003.
27. Wortis, H.H. Immunological responses of 'nude' mice. Clin Exp Immunol **8,** 305, 1971.
28. Rhee, S.H., Choi, J.Y., and Kim, H.M. Preparation of a bioactive and degradable poly(ε-caprolactone)/silica hybrid through a sol-gel method. Biomaterials **23,** 4915, 2002.
29. Rhee, S.H. Effect of molecular weight of poly(ε-caprolactone) on interpenetrating network structure, apatite-forming ability, and degradability of poly(ε-caprolactone)/silica nano-hybrid materials. Biomaterials **24,** 1721, 2003.
30. Costa, R.O.R., Lameiras, F.S., and Vasconcelos, W.L. Structural control in poly(butyl acrylate)-silica hybrids by modifying polymer-silica interactions). J Sol-Gel Sci Tech **27,** 343, 2003.
31. Costa, R.O.R., Pereira, M.M., Lameiras, F.S., and Vasconcelos, W.L. Apatite formation on poly(2-hydroxyethyl methacrylate)-silica hybrids prepared by sol-gel process. J Mater Sci Mater Med **16,** 927, 2005.
32. Craig, R.G., and Peyton, F.A. Elastic and mechanical properties of human dentin. J Dent Res **37,** 710, 1958.

Address correspondence to:
Ana Vallés-Lluch, Ph.D.
Center for Biomaterials and Tissue Engineering
Polytechnic University of Valencia
8E Building
Cno. de Vera s/n
Valencia 46022
Spain

E-mail: avalles@ter.upv.es

Received: February 10, 2010
Accepted: April 09, 2010
Online Publication Date: May 25, 2010